EJN
European Journal of Neuroscience

European Journal of Neuroscience, Vol. 28, pp. 1316–1328, 2008 doi:10.1111/j.1460-9568.2008.06442.x

NEUROSYSTEMS

Glial responses, neuron death and lesion resolution after intracerebral hemorrhage in young vs. aged rats

Jason K. Wasserman,[1,2] Helen Yang[1] and Lyanne C. Schlichter[1,2]
[1]Toronto Western Research Institute, University Health Network, Toronto Western Hospital, 399 Bathurst Street, Toronto, ON, Canada
[2]Department of Physiology, University of Toronto, Toronto, ON, Canada

Keywords: aged rats, astrocytes, dystrophic microglia, microglia, neuroinflammation, residual lesion, stroke

Abstract

Intracerebral hemorrhage (ICH) usually affects older humans but almost no experimental studies have assessed aged animals. We address how aging alters inflammation, neuron death and lesion resolution after a hemorrhage in the rat striatum. In the normal aged brain, microglia displayed a 'dystrophic' phenotype, with shorter cellular processes and large gaps between adjacent cells, and there was more astrocyte reactivity. The ICH injury was monitored as hematoma volume and number of dying neurons at 1 and 3 days, and the volume of the residual lesion, ventricles and lost tissue at 28 days. Inflammation at 1 and 3 days was assessed from densities of microglia with resting vs. activated morphologies, or expressing the lysosomal marker ED1. Despite an initial delay in neuron death in aged animals, by 28 days, there was no difference in neuron density or volume of tissue lost. However, lesion resolution was impaired in aged animals and there was less compensatory ventricular expansion. At 1 day after ICH, there were fewer activated microglia/macrophages in the aged brain, but by 3 days there were more of these cells at the edge of the hematoma and in the surrounding parenchyma. In both age groups a *glial limitans* had developed by 3 days, but astrocyte reactivity and the spread of activated microglia/macrophages into the surrounding parenchyma was greater in the aged. These findings have important implications for efforts to reduce secondary injury after ICH and to develop anti-inflammatory therapies to treat ICH in aged humans.

Introduction

Intracerebral hemorrhage (ICH) is a catastrophic form of stroke caused by rupture of a blood vessel in the brain, with subsequent accumulation of blood in the parenchyma (Rincon & Mayer, 2004). ICH accounts for 10–30% of hospital admissions for stroke and is much more devastating than ischemic stroke, with ~50% mortality by 6 months and only ~20% of survivors regaining functional independence (Mayer & Rincon, 2005). Unfortunately, despite a number of preclinical studies reporting positive results, no drugs have been translated into human treatments (Badjatia & Rosand, 2005). An important concern is that ICH is mainly a disease of the elderly (Collins *et al.*, 2003), in whom there are increases in the major predisposing factors: chronic hypertension and amyloid angiopathy (O'Donnell *et al.*, 2000; Ariesen *et al.*, 2003). Despite this, experimental models have almost exclusively used young animals. This significant gap in our understanding of ICH undoubtedly limits the translation of preclinical studies into potential human treatments.

During ICH, rapid blood entry into the brain causes mechanical disruption and death of neurons trapped inside the matrix of the hematoma. In the parenchyma adjacent to the hematoma (the 'perihematomal' tissue), neuron death continues for 2–3 days (Felberg *et al.*, 2002; Wasserman & Schlichter, 2007a). This neurodegeneration is thought to result from apoptosis, due to toxic factors diffusing out of the hematoma, and to activation of inflammatory cells that begin to accumulate hours after the ICH onset (Xue & Del Bigio, 2001; Wasserman & Schlichter, 2007a). In young animals, experimental therapies that decrease the inflammatory response are associated with less blood–brain barrier disruption and cell death, and improved functional outcome (Masada *et al.*, 2001; Mayne *et al.*, 2001a,b; Peeling *et al.*, 2001; Power *et al.*, 2003; Wang *et al.*, 2003; Wang & Tsirka, 2005b; MacLellan *et al.*, 2006; Wasserman *et al.*, 2007). However, as very little is known about the nature of the inflammatory response in older animals, it is risky to proceed to preclinical trials.

The two experimental studies that have addressed ICH in the aged brain used the autologous blood injection model and showed worse functional outcomes in aged animals but presented limited information on glial responses (Gong *et al.*, 2004). Aged senescence-prone mice had more microglia around the hematoma at 3 days (Lee *et al.*, 2006) but their activation status was not determined. Aged rats had fewer reactive astrocytes and more microglia (Gong *et al.*, 2004) but their location and activation state were not indicated. Neither study defined the spatial and temporal relationship between microglia and secondary neuron death or the

Correspondence: Dr Lyanne C. Schlichter, [1]Toronto Western Research Institute, as [1]above.
E-mail: schlicht@uhnres.utoronto.ca

Received 28 February 2008, revised 25 July 2008, accepted 5 August 2008

relationship between early neuronal injury and long-term brain atrophy. To address these issues, and for comparison with the autologous blood model, we used the collagenase injection model to ask whether aging affects early hematoma development, microglial activation, neuron death, the development of a *glial limitans*, and later injury resolution. We show that aging affects almost all of these aspects of development and resolution of the ICH lesion.

Materials and methods

Animals

Male Sprague–Dawley rats (Charles River, MA, USA) were housed in pairs, maintained under a 12-h light–dark cycle, and given food and water *ad libitum.* All procedures were approved by the University Health Network animal care committee, in accordance with guidelines established by the Canadian Council on Animal Care. Young animals were used at 3–4 months and aged rats were 22 months at the time of surgery. For aged animals, rats were purchased at 12 months old and aged in our animal facility. When raised under similar conditions, the life span of Sprague–Dawley rats has a mean of ∼25 months and a maximum of ∼30 months (Masoro, 1980). Therefore, the older rats used in this study represent late middle age to early old age, which corresponds well with the average age at which humans experience ICH, ∼60 years old (Collins *et al.*, 2003). No rats (young or aged) died as a result of the surgery or ICH induction, but because five animals died of age-related complications before reaching 22 months we did not attempt to induce ICH in older rats.

Induction of intracerebral hemorrhage

Intracerebral hemorrhage was induced in the striatum using a method modified from Rosenberg and colleagues (Rosenberg *et al.*, 1990; MacLellan *et al.*, 2004; Wasserman & Schlichter, 2007a). Rats were anesthetized using isofluorane (3% induction, 1.5% maintenance) and placed in a stereotaxic frame (n = 19 young, 19 aged). In addition, Xylocaine (0.1 mL; AstraZeneca, Mississauga, ON, Canada) was injected subcutaneously into the scalp to minimize pain from the incision. Under aseptic conditions, a 1-mm-diameter burr hole was drilled in the skull (0.2 mm anterior and 3 mm lateral to bregma) and a 30-gauge needle lowered into the right caudate–putamen (6 mm ventral from the skull surface). A micropump (Micro4; World Precision Instruments, Sarasota, FL, USA) delivered 0.1 U of bacterial type IV collagenase (Sigma, Oakville, ON, Canada) in 0.5 μL saline at 250 nL/min, after which the needle was left in place for 5 min to prevent solution reflux. We used less collagenase than previously used in order to produce a smaller hematoma and reduce the likelihood of ICH-induced mortality in the aged rats. Sham-operated animals (n = 12) underwent the same surgical procedure, but without collagenase in the injected saline. For all surgeries, core body temperature was maintained at 36.5 °C using an electric heating pad throughout surgery and recovery. Animals regained consciousness within 10 min. Although all animals displayed obvious behavioral deficits within hours of ICH onset (i.e. ipsilateral turning bias), their ability to eat, drink and clean themselves was not impaired. After ICH induction, all animals lost a similar proportion of their weight; i.e. ∼10% for young and ∼12% for aged animals after 3 days. Then, by the end of the 28-day study period, the young animals had increased in weight by ∼32% (from 388 ± 14 to 513 ± 25 g) whereas aged rats lost a further 3% of their weight (from 586 ± 51 to 569 ± 58 g).

Tissue preparation

After ICH, five animals for each experimental group (four each for naïve young and aged animals) were killed by an overdose of isofluorane at 1, 3 or 28 days after ICH onset. They were perfused through the heart with 100 mL PBS, followed by 60 mL of fixative (4% paraformaldehyde and 2% sucrose in PBS, pH 7.5). Dissected brains were stored in the same fixative at 4°C overnight, followed by 10% sucrose for 24 h and 30% sucrose for 48 h. Fixed brains were cut coronally through the needle entry site, and at 4 mm anterior and 4 mm posterior to that plane. Frozen brain sections (16 μm thick) were made using a cryostat (JungCM 3000; Leica, Richmond Hill, ON, Canada) and stored at −80°C until used.

Assessing neuron death

Neuron death was quantified using Fluoro-Jade B, which selectively labels degenerating neurons (Schmued & Hopkins, 2000). Frozen brain sections were prepared by sequential immersion in 100% ethanol for 3 min, 70% ethanol for 1 min, dH_20 for 1 min, 0.06% potassium permanganate (in dH_20) for 15 min and then dH_20 for 1 min. Then, a 0.001% solution of Fluoro-Jade B (in dH_20 containing 0.1% acetic acid) was applied for 30 min, after which the sections were rinsed three times in dH_20, dried at room temperature and examined using a confocal microscope (Zeiss LSM 510 META, Oberkochen, Germany) and a 25× objective lens with a numerical aperture of 0.5.

Immunofluorescence

Neurons, astrocytes and microglia/macrophages were identified with antibodies against NeuN (mouse monoclonal, 1 : 100; Chemicon, Temecula, CA, USA), glial fibrillary acidic protein (GFAP; mouse monoclonal, 1 : 300; Sigma), and ionized calcium-binding adaptor molecule 1 (Iba1; rabbit polyclonal, 1 : 1000; Wako, Japan), respectively. Highly activated phagocytic microglia/macrophages were identified using an antibody directed against the lysosomal marker ED1 (mouse monoclonal, 1 : 250; Serotec, Raleigh, NC, USA). The secondary antibodies were FITC-conjugated donkey antimouse or Cy3-conjugated donkey antirabbit, as required. Frozen brain sections were incubated with a primary antibody for 24 h at 4 °C, followed by a secondary antibody for 2 h, with washes in PBS between successive steps (three times, 5 min each). The primary antibody was omitted for negative controls. All slides were examined with the confocal microscope (using 10×, 25× and 63× objective lenses with numerical apertures of 0.5, 0.8 and 1.2, respectively), and fluorescence images were processed using ImageJ software (version 1.33k, NIH) with background subtraction based on a threshold set in advance by the imaging software.

Cell counts

For each animal (one n-value), cell counts were made on individual confocal images (not z-stacks) and then average cell densities were calculated over all 12–15 regions (i.e. four or five per section times three sections). The results are then reported as the mean ± SD for n animals.

Naïve animals

To test for differences in neuron or microglia densities between normal young and aged animals, we quantified cells labeled with NeuN or

Iba1 in naïve animals (n = 3 per group) using an unbiased sampling protocol. Cell counts were made by an observer blinded to the age of the animal and compared with counts made with the automated ImageJ analysis software. For each animal, cells were counted in three coronal sections along the length of the striatum, and in five preselected nonoverlapping regions (125 × 125 μm) per section.

Dying neurons and inflammatory cells

The same unbiased sampling procedure was used to quantify the number of cells labeled with Fluoro-Jade, Iba1 or ED1 in the perihematomal tissue. Cell counts were made on individual confocal images by an observer blinded to the treatment, with automated counting using ImageJ software. To assess changes occurring throughout the injury at 1 or 3 days after ICH onset, three coronal sections were taken from each animal for each marker (nine sections per brain) using anterior (+1 mm), middle (−1 mm) and posterior (−2 mm) locations with respect to the hematoma. For each section, cells were counted in four preselected regions around the circumference of the hematoma, as illustrated in Fig. 1, for a total of 12 regions per animal. Within each region, Iba1-positive cells were also categorized by morphology (see Fig. 5B) as ramified (long, thin multi-branched processes, small cell body), activated (short, thick processes, small cell body) or macrophage-like (large cell body, no processes). To unambiguously count Iba1- or ED1-labeled cells, cell bodies rather than cell processes were counted. This was straightforward for activated (rounded up) cells (e.g. Figs 7 and 8), and for ramified microglia it was possible to distinguish their cell bodies, which were thicker than the processes emanating from them.

Striatal neuron loss was assessed at 28 days after ICH, with some modification of well-established procedures (Felberg *et al.*, 2002; MacLellan *et al.*, 2008). NeuN-positive cells were counted using ImageJ software in three coronal sections per animal (+1, −1, and −2 mm from the hematoma, as above). For each animal, cells were counted in five nonoverlapping 125 × 125 μm regions in three separate sections, for a total of 15 locations per animal (see Fig . 5E).

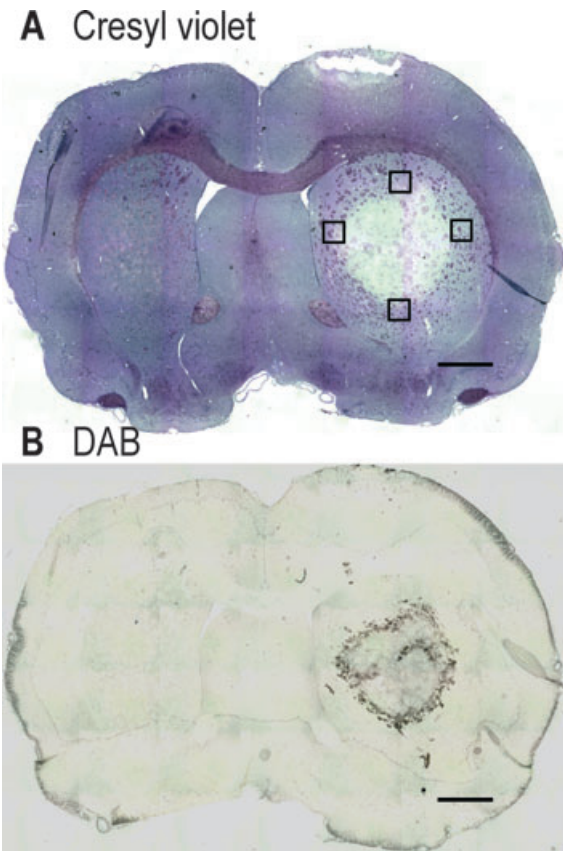

FIG. 1. Example of a typical collagenase-induced hematoma and the sampling procedure. Representative 16-μm-thick coronal sections through the middle of the hematoma in a young rat at 1 day after ICH onset. The images were compiled from smaller, higher magnification images made with a Leica DMRB microscope and processed with Virtual Slice software (MBF Bioscience, VT, USA). (A) This section was stained with Cresyl violet. The black boxes indicate the approximate sizes and positions of regions in which cells were counted and averaged after labeling with Fluoro-Jade B, or antibodies against Iba1 and ED1 in subsequent figures. Three coronal sections were sampled for each animal, representing the anterior, middle and posterior portions of the hematoma. (B) Staining with DAB shows blood inside the brain parenchyma. Scale bars, 1 mm.

Morphometric analysis

The volumes of the hematoma, residual lesion, tissue loss and ventricular expansion were determined using well established procedures (Felberg *et al.*, 2002; Wasserman & Schlichter, 2007a; MacLellan *et al.*, 2008) but with some modification. Frozen brain sections (16 μm thick) were taken every 200 μm, starting at +2 mm and extending to −4 mm with respect to bregma. In order to build a complete brain image, a Leica DMRB stereology microscope was used to take high resolution images, which were then stitched together using Virtual Slice software. In each stitched image the region of interest was delineated by hand by an observer blinded to the age of the animal. Volumes of interest were calculated by averaging the appropriate cross-sectional area over all sections, and multiplying by the distance between sections (200 μm in this study) and number of sections (usually 20–25). The hematoma volume was determined at 1 day after ICH onset by staining frozen brain sections with 3,3′-diaminobenzidine tetrahydrochloride (DAB) containing a metal enhancer (Sigma; D0426), which reacts with hemoglobin to form a blue–black product while blood-free tissue remains almost clear. This method is preferable to homogenizing the whole brain; i.e. the same brain can be used for histochemistry, thus conserving expensive, hard-to-obtain aged tissue. The hematoma volume was calculated as: (average DAB-stained area) × (200 μm) × (number of sections). Tissue loss, ventricular expansion and residual lesion volume were determined in Cresyl Violet-stained frozen sections at 28 days after ICH onset. Acetic acid was omitted from the solution in order to stain all neuropil. The volume of tissue lost was the difference between the volume of the contralateral striatum and the remaining volume of the ipsilateral striatum, which was calculated as: (average area of striatum − average area of damage) × (200 μm) × (number of sections). The volume of ventricular expansion was the difference between the volume of the ipsilateral and contralateral ventricles, where the volume of each ventricle was calculated as: (average area of the ventricle) × (200 μm) × (number of sections). The volume of the residual lesion was calculated as: (average area of damage) × (200 μm) × (number of sections).

Statistical analyses

Where appropriate, data are expressed as the mean ± SD for the number of animals indicated. For all statistical analyses, one-way ANOVA was followed by Bonferroni's correction, with $P < 0.05$ considered significant.

Results

Glial changes with normal brain aging

To assess whether normal aging causes differences in the density of neurons or microglia, immunostaining was performed on frozen brain sections from naïve young and aged rats (n = 3 each), and neurons were identified in the striatum by nuclear staining with anti-NeuN antibody (Fig. 2A). There was no difference in neuron density between young (1073 ± 42 per mm^2) and aged (1054 ± 44 per mm^2) rats and, importantly, no Fluoro-Jade-positive degenerating neurons were detected in either age group. However, there were striking age-related differences in the microglial cells (Fig. 2B and C). In young animals, they were much more ramified, displayed multiple long, thin processes, and thus occupied a large territory. In the aged animals the processes were shorter and thicker, hence large gaps appeared between the microglial cells (see high magnification images in Fig. 2C). Despite this dramatic difference in morphology, there was no difference in the density of Iba1-stained microglia, which was 162 ± 14 cells per mm^2 in young and 153 ± 19 per mm^2 in aged rats. The astrocytes of young and aged rats also differed (Fig. 2D). In the striatum of young animals, staining for glial fibrillary acidic protein (GFAP) was most intense in cells that were adjacent to blood vessels. In the aged brain, GFAP was observed throughout the striatum, and many astrocytes displayed a reactive phenotype with long, prominent processes.

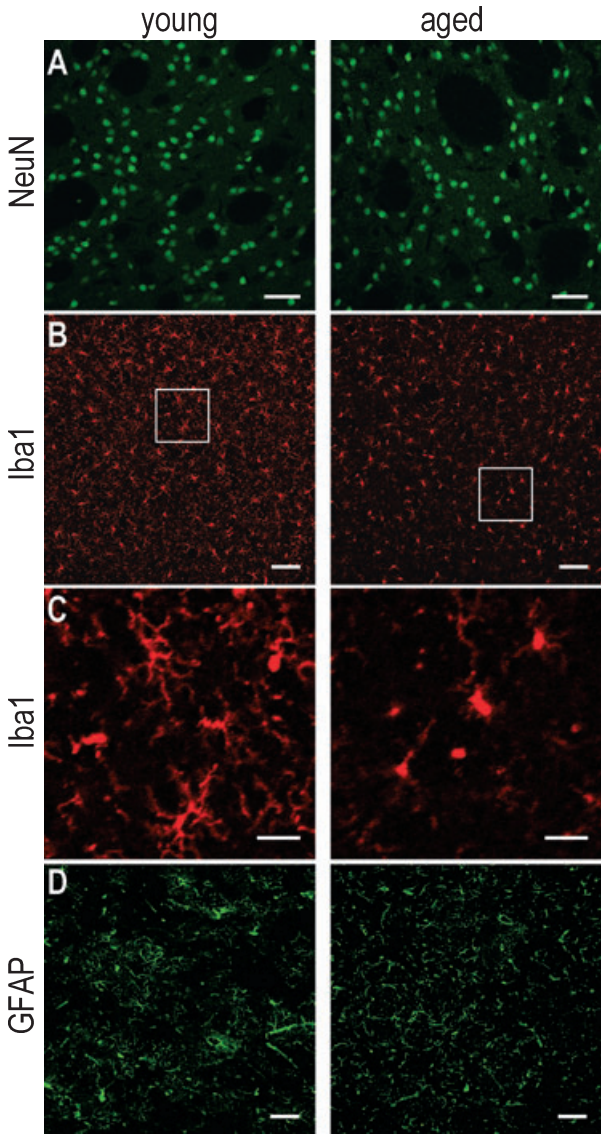

FIG. 2. Neurons, microglia and astrocytes in the striatum of naïve young and aged rats. Representative confocal images from antibody labeled 16-μm-thick frozen sections (three animals from each age group were examined). (A) Neuronal nuclei were labeled with an anti-NeuN antibody and FITC-conjugated donkey antimouse secondary antibody. (B) Microglia were labeled with an anti-Iba1 antibody, which recognizes the ionized calcium-binding adaptor molecule 1 and a Cy3-conjugated donkey antirabbit secondary antibody. (C) Higher magnification images of the areas in the white boxes in panel B. Note that Iba1-labeled microglia in the aged animal had fewer and shorter processes, and that large gaps were present between adjacent cells. (D) Astrocytes were labeled with an anti-GFAP antibody and a FITC-conjugated donkey antimouse secondary antibody. Note the widespread expression of GFAP in the aged animal compared with the primarily perivascular staining in young animals. Scale bars, 50 μm (A), 100 μm (B and D) and 25 μm (C).

Hematoma development and neuron loss after ICH

In both young and aged rats, injection of collagenase into the striatum produced a hematoma that was largely limited to the anterior portion of the striatum, most notably the head of the caudate (Fig. 3A). By

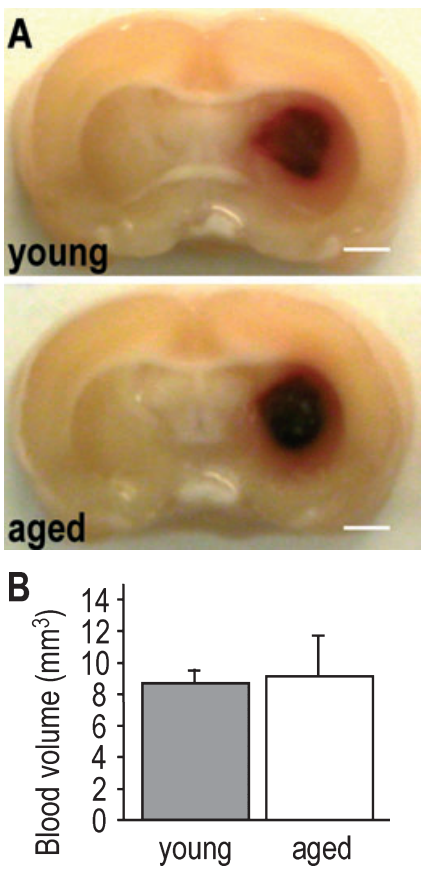

FIG. 3. Hematoma development after intracerebral hemorrhage. (A) Representative images of unstained 16-μm-thick coronal sections taken through the middle of the hematoma at 1 day after ICH onset. The hematoma in both young and aged rats was largely limited to the anterior portion of the striatum in the caudate, with some extension towards the ventricle. Diffuse blood can be seen in the striatum surrounding the hematoma. (B) The volume of the hematoma was determined at 1 day after ICH onset by staining with DAB. Each section was analyzed with ImageJ, and the hematoma volume was computed as: (average area of DAB staining) × (200 μm distance between sections) × (number of sections). Values are expressed as mean ± SD, n = 5 per group; n.s. Scale bars, 1 mm.

1 day after ICH onset, the hematoma compressed the ipsilateral ventricle and increased the volume of the ipsilateral hemisphere. DAB staining of blood (Fig. 3B) showed no difference in the hematoma volume, which was 8.7 ± 0.9 mm^3 in young and 9.1 ± 2.6 mm^3 in aged animals (five rats per group).

We recently observed delayed neuron death in the parenchyma immediately adjacent to the hematoma (perihematomal tissue) between 1 and 3 days after ICH onset (Wasserman & Schlichter, 2007a). Here, we used Fluoro-Jade B to quantify degenerating neurons (Schmued & Hopkins, 2000) in the striatum. In control saline injected animals (no ICH), no Fluoro-Jade-positive cells were seen in the striatum of either age group (a few were present along the needle entry track). In collagenase-injected animals of both age groups (Fig. 4A), many Fluoro-Jade-positive neurons were seen by 1 day after ICH within the hematoma and in a 100- to 200-μm-wide perihematomal band. Surprisingly, the density of Fluoro-Jade-positive cells was higher in young (398 ± 67 per mm^2) than in aged (318 ± 24 per mm^2; $P < 0.05$, $n = 5$ per group; Fig. 4B) rats. By 3 days after ICH, the density of Fluoro-Jade-positive cells decreased and there was no difference between young (135 ± 34 per mm^2) and aged (154 ± 26 per mm^2; $n = 4$ per group; Fig. 4B) animals. Consistent with our recent study on young rats (Wasserman & Schlichter, 2007a), no

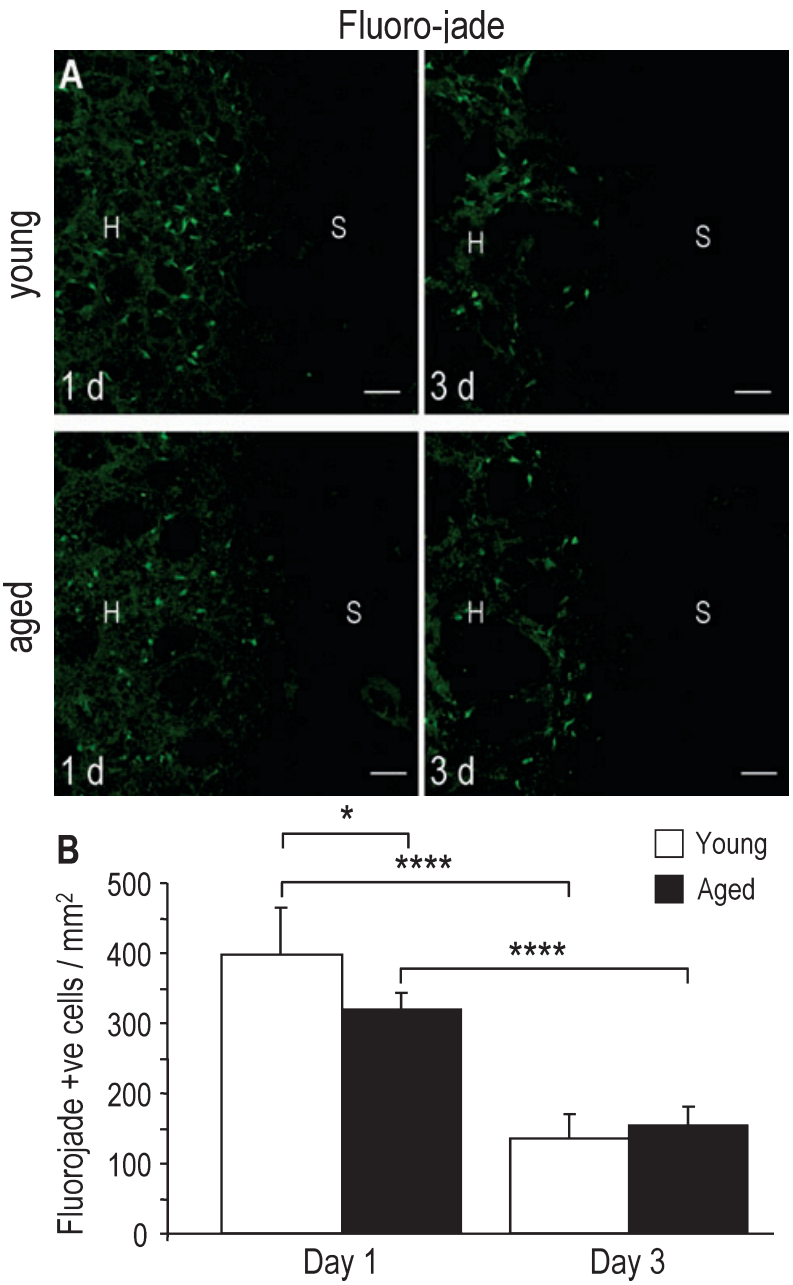

FIG. 4. Effect of aging on neuron death after ICH. (A) Representative confocal images of 16-μm-thick Fluoro-Jade B-labeled sections at 1 day after ICH onset, showing degenerating neurons. In both young and aged rats, most of the Fluoro-Jade-positive neurons were in the hematoma (H) and perihematomal tissue. Note the sharp delineation between the hematoma and the surrounding striatum (S) which lacked Fluoro-Jade-positive cells. (B) Densities of degenerating, Fluoro-Jade (FJ)-positive neurons in the striatum of young and aged rats at 1 and 3 days after ICH. Values are mean ± SD; *$P < 0.05$, ****$P < 0.001$; $n = 5$ per group. Scale bars, 50 μm.

degenerating neurons were seen in the surrounding parenchyma in either age group at 1 or 3 days.

Striatal neuron loss was estimated by counting the number of NeuN-positive cells along the rostral–caudal axis of the hematoma 28 days after ICH onset (Fig. 5A). The preselected regions used for cell counting in each section are illustrated in Fig. 5B. Consistent with a previous reports on young animals (Felberg *et al.*, 2002), the neuron density in young and aged animals was the same in the contralateral striatum as in naïve animals, and the same in the surrounding ipsilateral striatum of ICH animals (i.e. 1091 ± 47 per mm^2 in young and 1063 ± 56 per mm^2 in aged animals; $n = 5$ per group), and no surviving neurons were seen in the hematoma (more debris was present in most aged animals). By 28 days after ICH, the ipsilateral striatum of both age groups had fewer surviving neurons (Fig. 5C; 832 ± 50 per mm^2 for young, 787 ± 63 per mm^2 for aged) but there was no difference between young and aged animals. Thus, despite the early difference in numbers of dying neurons at the edge of the hematoma (Fig. 4), the same number of neurons was lost in both age groups by 28 days and there was no loss in the surrounding parenchyma.

Hematoma resolution and tissue loss

Lesion resolution after a stroke results from removal of dead tissue by phagocytes that are derived primarily from activated microglia (Schilling *et al.*, 2005). Based on reports that aged microglia are functionally impaired (Streit *et al.*, 2004; Simmons *et al.*, 2007; Lopes *et al.*, 2008) and less responsive to damage, we assessed whether lesion resolution after ICH differs with age. The volumes of the

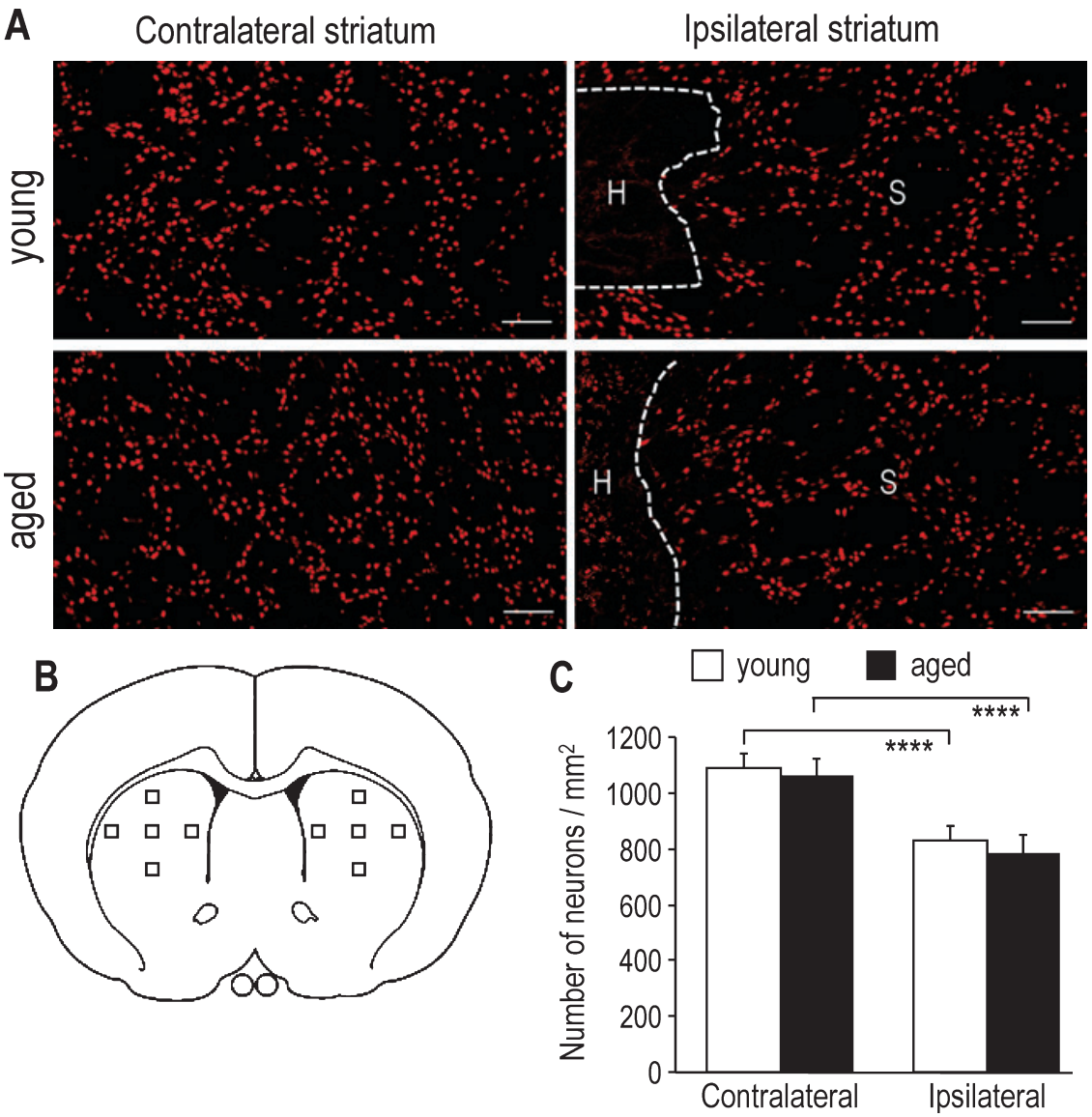

FIG. 5. Effect of aging on neuron loss in the striatum after ICH. (A) Representative confocal images, 16-μm-thick sections, at 28 days after ICH onset. Neuron nuclei were labeled with anti-NeuN antibody and donkey antimouse Cy3 secondary antibody. Inside the hematoma (H) there were no intact neurons in either age group, but NeuN-stained neuronal debris remained in the aged animals. NeuN staining in the striatum surrounding (S) the hematoma was similar to the contralateral striatum. (B) The boxes represent the five preselected regions of the striatum used for counting neurons in each of three coronal sections and calculating neuron loss. (C) Neuron densities in the striatum of young and aged rats at 28 days after ICH. Young and aged animals showed significant neuron loss in the ipsilateral striatum, with no difference in extent between the age groups. Values are mean ± SD; ****$P < 0.001$; $n = 5$ per group. Scale bars, 100 μm.

residual lesion, lost tissue and ventricular expansion were measured at 28 days after ICH onset in Cresyl violet-stained frozen brain sections from the entire rostral–caudal axis of the lesion (Fig. 6). Blood was no longer visible, and the residual lesion was considerably smaller than the original hematoma in both age groups (compare Fig. 6 with Fig. 1). Note the expansion of both ventricles in aged animals, owing to the brain atrophy that occurs during normal aging. Ventricular expansion on the ipsilateral side, which is often used as a surrogate marker of brain atrophy (Felberg *et al.*, 2002), was smaller in aged than young animals. At the position where the hematoma was largest, the lesion appeared as a fluid- and debris-filled cyst. In young animals the residual lesion was a thin scar in most brain sections, while in aged rats it usually appeared as a prominent round cavity. At higher magnification (Fig. 6A, right panels), there was a sharp delineation between the cyst and surrounding parenchyma in both age groups. There was no difference in the volume of tissue lost (Fig. 6B), which was 9.4 ± 1.4 mm^3 in young and 8.8 ± 1.2 mm^3 in aged animals. However, the volume of the residual lesion was ~50% smaller in young animals (1.6 ± 0.21 mm^3 vs. 3.4 ± 0.3 mm^3; $P < 0.001$; Fig. 6C), and young animals had more ventricular expansion (6.5 ± 1.1 mm^3) than the aged (4.2 ± 0.6 mm^3; $P < 0.001$; Fig. 6D). There was no age-related difference in the amount of striatal atrophy

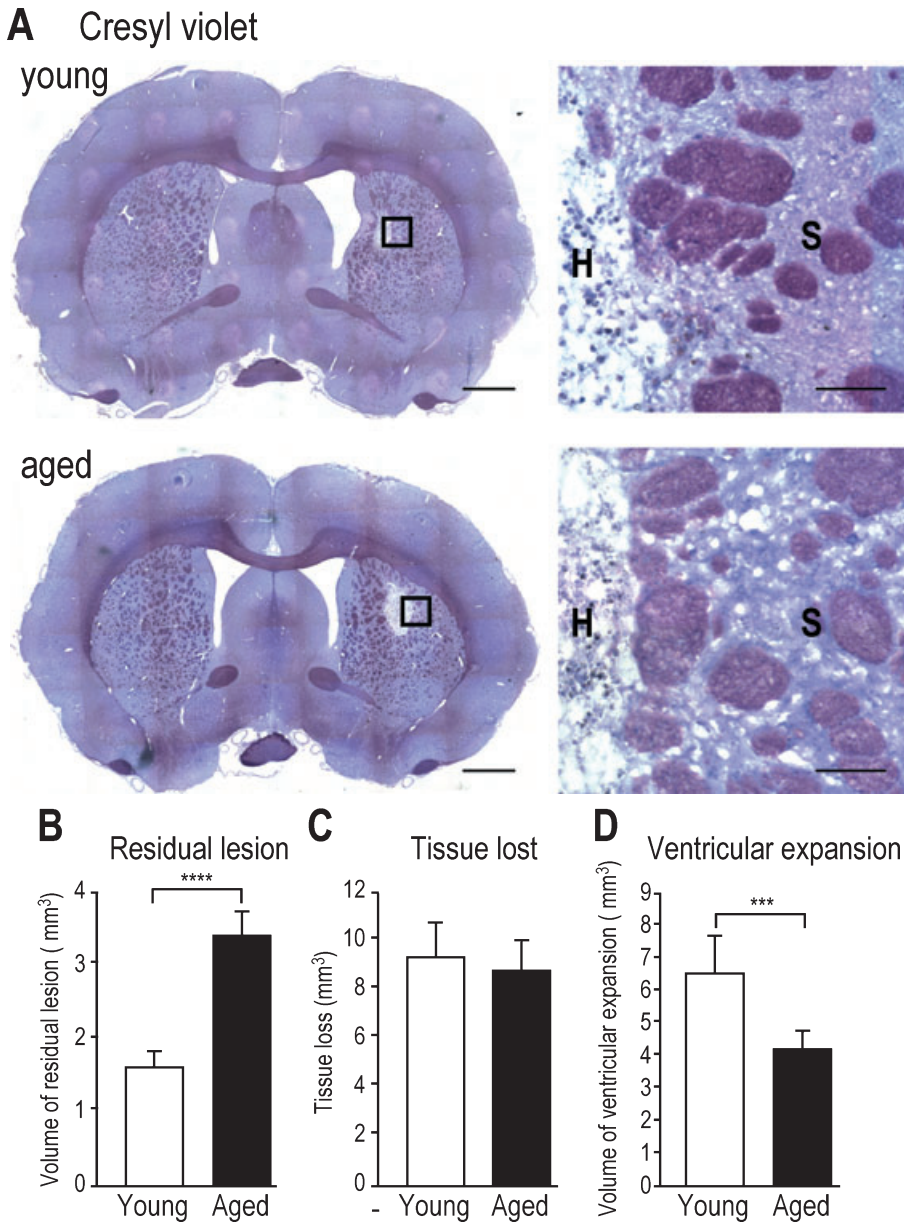

FIG. 6. Resolution of the lesion. At 28 days after ICH onset, brain sections were taken every 200 μm through the entire rostral–caudal axis of the hematoma and stained with Cresyl violet. (A) A representative 16-μm-thick section is shown for each age group. Aged rats show a prominent residual lesion and lack of ventricular expansion on the injured side. The regions inside the boxes are shown at higher magnification in the right panels. Note the sharp delineation between the hematoma (H) and the surrounding striatum (S). (B) The residual lesion volume was calculated as described in Materials and methods. (C) The volume of tissue lost was the difference between the volume of the contralateral striatum and remaining volume of the ipsilateral striatum (see Materials and methods). (D) The volume of ventricular expansion was the difference between the volume of the ipsilateral and contralateral ventricles (see Materials and methods). All values are expressed as mean ± SD; ***$P < 0.005$, ****$P < 0.001$; $n = 5$ per group. Scale bars, 1 mm (left), 100 μm (right).

(i.e. contralateral vs. ipsilateral striatal volumes), and in both age groups it was largely accounted for by the volume of ventricular expansion, which is consistent with a previous report (Felberg *et al.*, 2002). Specifically, the volume of striatal atrophy was 7.6 ± 1.2 mm^3 and the volume of ventricular expansion was 6.5 ± 1.1 mm^3 in young animals while, in aged animals, the volume of striatal atrophy was 5.5 ± 1.3 mm^3 and ventricular expansion was 4.2 ± 0.6 mm^3. Together, these data demonstrate that young and aged animals lost the same volume of tissue after ICH, but lesion resolution was impaired in aged animals.

Effects of aging on the microglial response after ICH

The prominent microglial response that occurs after ICH is characterized by transformation of ramified cells into an activated phenotype that can become indistinguishable from peripheral macrophages (illustrated in Fig. 7B). At 1 day after ICH onset (Fig. 7A), activated microglia were present at the edge of the hematoma and in the surrounding striatum of both young and aged animals. By 3 days, both age groups showed a prominent band of activated microglia and macrophage-like cells at the edge of the hematoma, and an increase in the number of activated microglia in the surrounding striatum. However, the band of activated microglia/macrophages was wider in aged animals and these cells extended further into the surrounding striatum.

The phenotypic classification (illustrated in Fig. 7B) was used to quantify densities of ramified microglia, activated microglia and macrophage-like cells at 1 and 3 days after ICH onset (Fig. 7C). There were several differences between young and aged animals ($n = 5$ per group). At 1 day, young animals had more activated microglia (133 ± 15 vs. 98 ± 20 per mm^2; $P < 0.001$) and macrophage-like cells (56 ± 17 vs. 36 ± 12 cells per mm^2; $P < 0.005$). In contrast, at 3 days, young animals had fewer activated microglia (243 ± 43 vs. 304 ± 49 per mm^2; $P < 0.005$) and macrophage-like cells (263 ± 42 vs. 327 ± 42 per mm^2; $P < 0.005$). There were very few ramified microglia at either 1 or 3 days, and no differences between the age groups.

When microglia, macrophages and neutrophils become phagocytic, expression of the lysosomal marker ED1 is increased. Not surprisingly, ED1-positive cells were not detected in the striatum of naïve young or aged rats (present study) or in the healthy aged rat brain (Kullberg *et al.*, 2001). In both young and aged rats (Fig. 7A and Fig. 8) we observed many ED1-positive, highly activated microglia/macrophages at the edge of the hematoma and a few scattered throughout the surrounding striatum as early as 1 day after ICH onset whereas, at 3 days, most were at the edge of the hematoma. At 1 day, the density of ED1-positive cells (Fig. 7B) did not differ between young (131 ± 24 cells per mm^2) and aged (125 ± 13 per mm^2) rats. At 3 days, ED-1 showed a similar distribution to Iba1 staining, with a wider band in aged animals and more ED-1-positive cells in aged (274 ± 37 cells per mm^2) than young (201 ± 30 cells per mm^2) animals.

Effects of aging on the development of a glial limitans after ICH

After acute brain injury, the lesion becomes separated from the surrounding parenchyma by a *glial limitans* comprised of reactive astrocytes and activated microglia/macrophages (Gehrmann *et al.*, 1992; Clark *et al.*, 1993; Lehrmann *et al.*, 1997). Because these cells contribute to the lesion resolution and plasticity in the surrounding parenchyma (Koeppen *et al.*, 1995), we examined the development of the *glial limitans* at 3 days after ICH. In both young (Fig. 9A) and aged (Fig. 9B) rats the lesion was delineated by a band of activated microglia/macrophages and, importantly, it was inside the band of reactive astrocytes. Based on the morphological criteria for microglial activation illustrated in Fig. 7, the higher magnification images in Fig. 9 (panels C and D) show that the microglia within ~600 μm of the lesion edge were activated in both age groups. There were three apparent differences between the age groups. In aged animals, activated microglia/macrophages were more diffusely distributed, with some in the surrounding parenchyma; the astrocytic border of the lesion was more clearly defined; and there appeared to be more GFAP reactivity in the parenchyma surrounding the hematoma.

Discussion

Although ICH most often affects older humans, surprisingly few experimental studies have used aged animals. By comparing young and aged rats, we provide new information concerning acute and longer term consequences of aging on the outcome after ICH, as follows. (i) Neuron death was delayed in aged animals. At 1 day after ICH there was less neuron death in the perihematomal tissue of aged animals, but by 3 days there was no difference and striatal neuron loss was the same at 28 days. (ii) Aging impaired the lesion resolution but did not affect the volume of brain tissue lost in the longer term (28 days). That is, the same amount of striatal tissue remained in both age groups, even though aged animals had a larger volume of residual lesion and less ventricular expansion. (iii) Aging affected the microglial activation response. In the striatum surrounding the hematoma, aged animals had fewer activated microglia and macrophage-like cells at 1 day after ICH, but more than young animals at 3 days. In addition, aged animals had more ED1-positive cells (a marker of phagocytic capacity) at 3 days. (iv) Aging affected the formation of the *glial limitans*. By 3 days, a prominent *glial limitans* formed in both groups but aged animals showed greater astrocyte reactivity and a greater spread of macrophage-like cells into the surrounding parenchyma. Together, our results show that aging did not increase neuron death after ICH; rather, it impaired the lesion resolution and delayed what ultimately became a more pronounced microglial/macrophage response.

Microglia maintain the delicate homeostasis of the brain, survey the environment and respond to environmental cues and brain damage (Nimmerjahn *et al.*, 2005). In the healthy adult brain, microglia are highly ramified and ideally positioned with their finely branched processes closely apposed to most, if not all, brain cells. However, this study supports the view that the protective ability of microglia becomes impaired in aged animals (Conde & Streit, 2006). For instance, microglia in aged rats had much fewer and shorter processes, which resulted in large gaps in the fields covered by these cells. The increased distance between the microglia and other brain cells will probably impair their ability to respond to diffusible pathological stimuli. Microglia with similarly aberrant morphologies (called 'dystrophic') have been reported in humans with Alzheimer's disease, where they are thought to reflect effects of cell senescence in the aged brain (Streit *et al.*, 2004). In that study it was proposed that the reduced phagocytosis of beta-amyloid by dystrophic microglia plays a role in disease progression.

Microglia are innate immune cells of the brain; they are activated by neuronal injury in order to remove cellular debris, and they support tissue repair and regeneration (Kreutzberg, 1996). However, the ability of microglia to exhibit both neuroprotective and neurotoxic properties

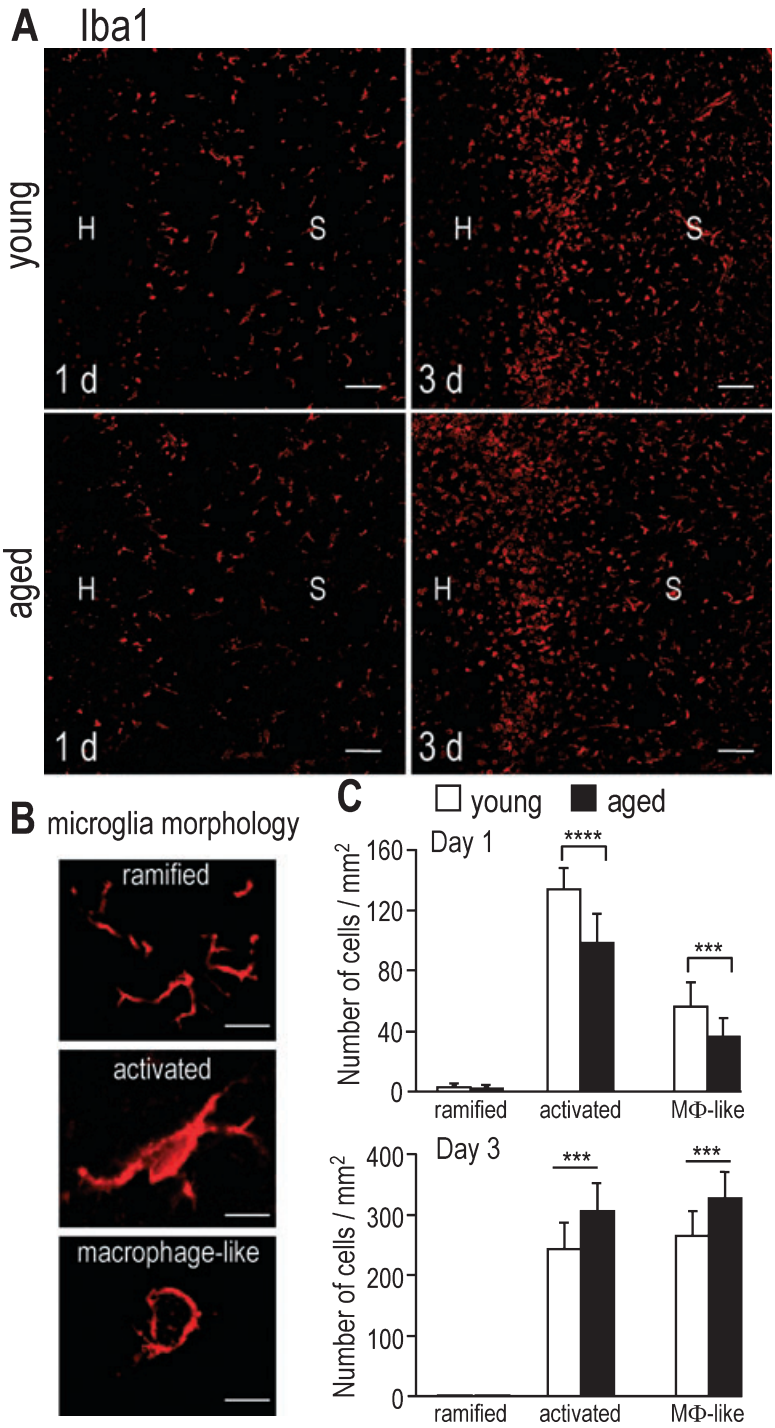

FIG. 7. Effect of aging on the microglial response after ICH. (A) Representative confocal images from antibody-labeled 16-μm-thick brain sections at 1 and 3 days after ICH onset. Microglia and macrophages were labeled with anti-Iba1, with a Cy3-conjugated donkey antirabbit secondary antibody. Note the cells lacking ramifications (illustrated in panel B) at the edge of the hematoma (H) and in the surrounding striatum (S) at 1 day. By 3 days macrophage-like cells formed a prominent band at the edge of the hematoma. (B) Higher magnification confocal images of Iba1-labeled cells, which were classified according to morphology as ramified, activated or macrophage-like. (C) Summary of microglia phenotypic activation state after ICH in young *vs.* aged rats. Iba1-labeled cells were counted in four regions around the circumference of the hematoma (sampling regions illustrated in Fig. 1) from three coronal sections for each animal, and classified according to the morphologies shown in panel B; MΦ, macrophage. Values are mean ± SD; $n = 5$ for each group. ***$P < 0.005$, ****$P < 0.001$. Scale bars, 100 μm (A), 15 μm (B).

has been demonstrated in numerous studies *in vivo* and using isolated cell cultures from young animals (Kreutzberg, 1996; Hanisch, 2002; Streit, 2002). *In vitro*, activated microglia can damage nearby neurons by producing reactive oxygen and nitrogen species and pro-inflammatory cytokines (Fordyce *et al.*, 2005; Kaushal *et al.*, 2007). The cause-and-effect relationship between neuron death and microglial activation has not been resolved *in vivo*. After ICH in young rats, secondary neuron loss in the perihematomal tissue correlates spatially and temporally with accumulation of activated microglia/macrophages that are producing interleukin-1β (Wasserman & Schlichter, 2007a;

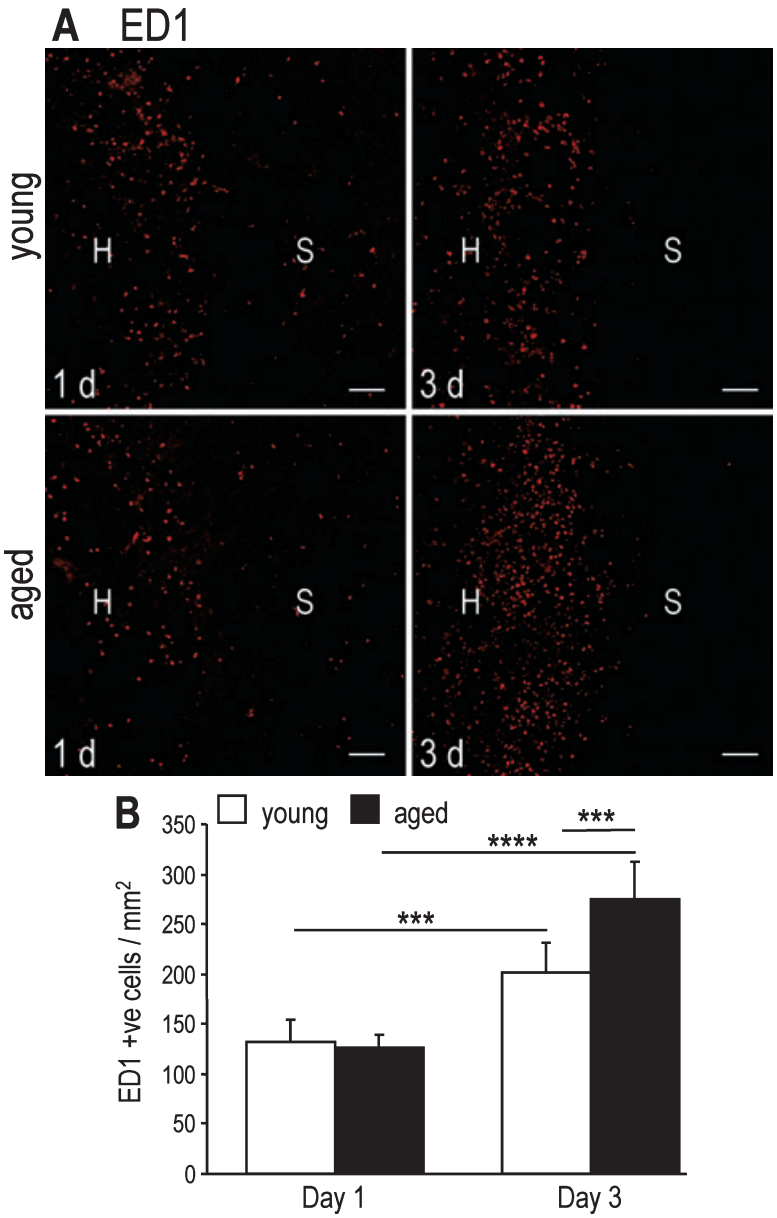

FIG. 8. Effect of aging on ED-1 expressing cells after ICH. (A) Representative confocal images from 16-μm-thick brain slices at 1 and 3 days after ICH. Sections were labeled with an antibody directed against the lysosomal marker ED1, with a Cy3-conjugated donkey antimouse secondary antibody. Note that ED1-labeled cells are present both at the edge of the hematoma (H) and in the surrounding striatum (S) at 1 day, but mainly in the band of activated microglia/macrophages at 3 days. (B) Densities of ED-1-positive cells after ICH in young vs. aged rats were calculated from cell counts in four regions around the circumference of the hematoma (as shown in Fig. 1) and from three coronal sections per animal. Values are mean ± SD; $n = 5$ for each group. ***$P < 0.005$, ****$P < 0.001$. Scale bars, 100 μm.

Wasserman *et al.*, 2007). Moreover, decreased microglia/macrophage accumulation is associated with reduced neuron loss after ICH in young mice (Wang & Tsirka, 2005a,b). Here we found that, in aged rats, microglia in the perihematomal tissue were less activated and neuron death was decreased at 1 day after ICH onset. These observations are in accord with reports on two other models of brain injury: a delay in neuron death in aged animals has been reported for NMDA-induced excitotoxicity and for transient focal ischemia (He *et al.*, 2005; Castillo-Ruiz *et al.*, 2007). At present, no one has resolved whether reduced microglial activation in the aged brain results from neurons being less susceptible to damage or microglia being less sensitive to environmental cues, or both.

Here, we show that aged animals had increased microglial activation and a further spread of macrophage-like cells into the surrounding parenchyma at 3 days after ICH onset. At the same time point, aged animals had more inflammatory cells expressing ED1, a marker of highly activated microglia/macrophages (Damoiseaux *et al.*, 1994). These results are consistent with a study of ischemic stroke, in which more ED1-positive cells were observed in aged animals (Badan *et al.*, 2003). Importantly, we show for the first time that despite these changes in microglial activation with age there was no difference in the extent of neuron death in the perihematomal tissue (3 days after ICH), in the number of neurons lost in the striatum (28 days), or in the total volume of brain tissue lost (28 days). Taken together, these results suggest that increased microglial activation does not increase neuron death after ICH *in vivo*, despite the observations that activated microglia produce molecules capable of killing neurons *in vitro*. In order to elucidate the specific functions of the different

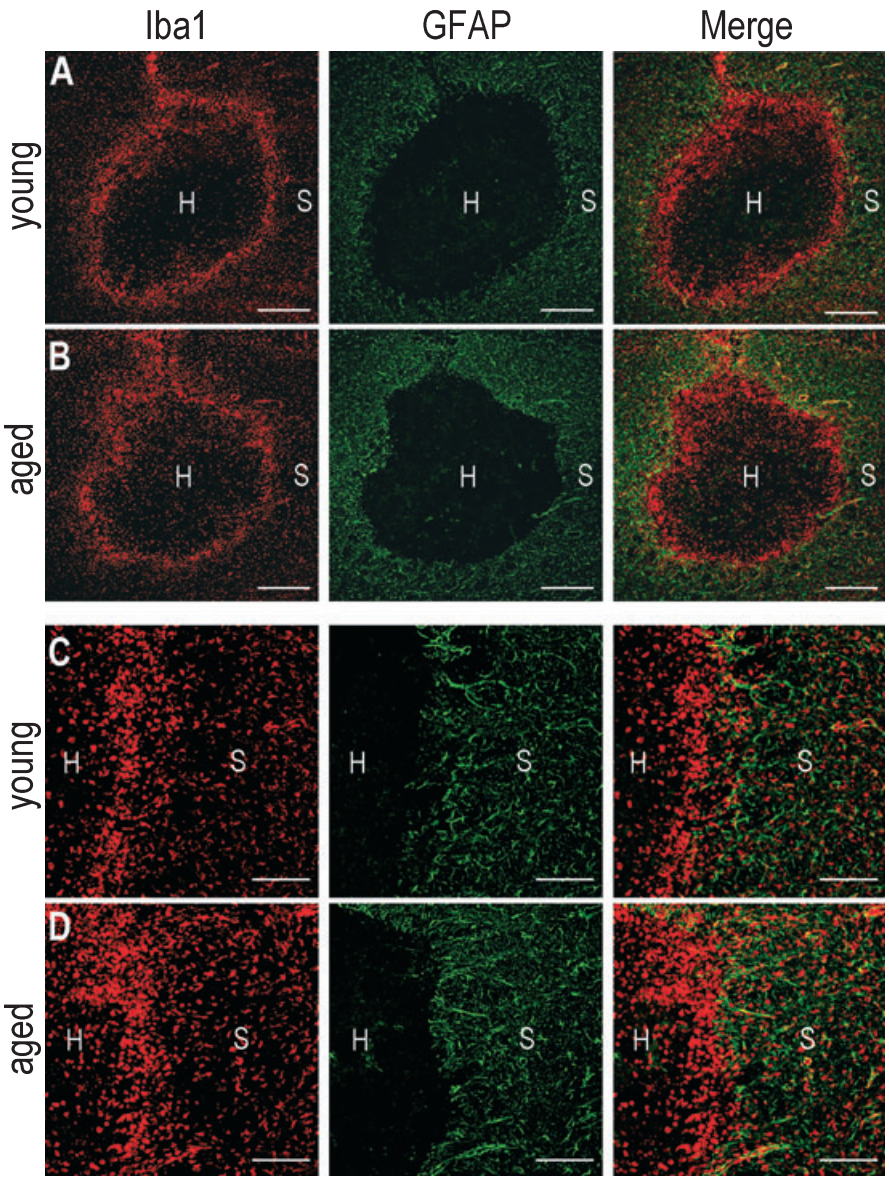

FIG. 9. Effect of aging on the development of a *glial limitans* after ICH. Representative confocal images from 16-μm-thick sections at 3 days after ICH onset (five animals from each age group were examined). Microglia and macrophages were labeled with an anti-Iba1 primary antibody and a Cy3-conjugated donkey antirabbit secondary antibody. Astrocytes were labeled with anti-GFAP antibody and a FITC-conjugated donkey antimouse secondary antibody. (A and B) Iba1 and GFAP labeling delineate a prominent *glial limitans* surrounding the hematoma (H) in young and aged animals. In aged animals (panel B), note the more diffuse distribution of Iba1 staining in the band at the edge of the hematoma, and increased GFAP reactivity in the surrounding striatum (S). (C and D) Higher magnification images of the border between the hematoma and surrounding striatum. Note that, in young animals, most of the Iba1-labeled cells with macrophage-like morphology are on the hematoma side of the astrocytic border while they are present in the surrounding striatum in aged animals. Scale bars, 500 μm (A and B), 200 μm (C and D).

phenotypes of activated microglia/macrophages in time, space and different-aged animals, it will be important in future to determine what molecules they produce.

The residual lesion size is important; in both rats and humans, it decreases within weeks after ICH and its size affects the prognosis. Larger lesion volumes correlate with poorer outcome in humans (Franke *et al.*, 1991; Castillo *et al.*, 2002), and therapies that promote lesion clearance improve the functional outcome in rats (Zhao *et al.*, 2007). Felberg *et al.* (2002) found that the initial hematoma volume correlated with the degree of brain atrophy at 100 days, and the loss of brain tissue was compensated for by an increase in ventricular volume. Here, we show that aged rats had larger residual lesions and less ventricular expansion at 28 days after ICH, even with the same initial hematoma size (1 day) and amount of tissue lost (28 days). No comparable studies have been reported for experimental ICH but our observations are consistent with studies of ischemic stroke, which showed decreased lesion resolution in aged animals (Futrell *et al.*, 1991; Popa-Wagner *et al.*, 1998). The present study suggests that while young and aged animals lose the same amount of tissue (as a consequence of neuron death), the infarct is not removed at the same rate, thus resulting in less atrophy and less ventricular expansion. Because activated microglia/macrophages contribute to injury resolution by surrounding the lesion and removing cellular debris, the simplest interpretation is that phagocytosis is impaired in the aged rats, as reported for 'dystrophic' microglia in aged animals (Streit, 2002; Fiala *et al.*, 2005). It is also possible that other aspects of aging; e.g. changes in microcirculation or nutrient status, contribute to the changes in lesion resolution. No cause–effect relationship has been

proven in any stroke model, nor can we rule out a contribution of the increased astrocyte reactivity at the edge of the lesion. That is, the *glial limitans* might have reduced lesion resolution by preventing activated microglia/macrophages from accessing the lesion. Increased astrocyte reactivity after ischemic stroke correlated with decreased regeneration and plasticity in the parenchyma adjacent to the infarct (Badan *et al.*, 2003). Thus, factors contributing to the poorer functional recovery of aged animals after ICH (Gong *et al.*, 2004) might include impaired lesion resolution and increased astrocyte reactivity.

In order to develop effective therapies to treat ICH, realistic molecular and cellular targets will need to be identified in both young and aged animals. The present results suggest that neuroprotection strategies are likely to have limited functional benefits in either age group because secondary neuron death (outside the hematoma) occurs only in a small band of parenchyma immediately adjacent to the hematoma. Instead, our finding that lesion resolution is impaired in aged animals suggests that strategies to enhance the beneficial activities of the innate immune system might improve functional recovery by promoting repair and regeneration. While an increased inflammatory response did not correspond with more neuron death in aged animals, we have recently found that activated microglia/macrophages contribute to blood–brain barrier disruption (Wasserman & Schlichter, 2007b) and to white matter damage in the tissue surrounding the hematoma (Wasserman and Schlichter, unpublished results). Based on the present results, future studies should focus on modulating the inflammatory response in aged animals in order to reduce damage early after ICH onset and promote long-term recovery.

Acknowledgements

We thank Drs J. Eubanks, L. Mills and E. F. Stanley for helpful comments on the work, and V. Kena-Cohen for critically reading the manuscript. Supported by grants to L.C.S. from the Heart & Stroke Foundation, Ontario Chapter (HSFO; NA5158, T5546, T6279), and scholarships to J.K.W. from the Peterborough K. M. Hunter Foundation and the Heart & Stroke Foundation, Ontario Chapter.

Abbreviations

DAB, 3,3′-diaminobenzidine tetrahydrochloride; GFAP, glial fibrillary acidic protein; Iba1, ionized calcium-binding adaptor molecule 1; ICH, intracerebral hemorrhage.

References

Ariesen, M.J., Claus, S.P., Rinkel, G.J. & Algra, A. (2003) Risk factors for intracerebral hemorrhage in the general population: a systematic review. *Stroke*, **34**, 2060–2065.

Badan, I., Buchhold, B., Hamm, A., Gratz, M., Walker, L.C., Platt, D., Kessler, C. & Popa-Wagner, A. (2003) Accelerated glial reactivity to stroke in aged rats correlates with reduced functional recovery. *J. Cereb. Blood Flow Metab.*, **23**, 845–854.

Badjatia, N. & Rosand, J. (2005) Intracerebral hemorrhage. *Neurologist*, **11**, 311–324.

Castillo, J., Davalos, A., Alvarez-Sabin, J., Pumar, J.M., Leira, R., Silva, Y., Montaner, J. & Kase, C.S. (2002) Molecular signatures of brain injury after intracerebral hemorrhage. *Neurology*, **58**, 624–629.

Castillo-Ruiz, M.M., Campuzano, O., Acarin, L., Castellano, B. & Gonzalez, B. (2007) Delayed neurodegeneration and early astrogliosis after excitotoxicity to the aged brain. *Exp. Gerontol.*, **42**, 343–354.

Clark, R.K., Lee, E.V., Fish, C.J., White, R.F., Price, W.J., Jonak, Z.L., Feuerstein, G.Z. & Barone, F.C. (1993) Development of tissue damage, inflammation and resolution following stroke: an immunohistochemical and quantitative planimetric study. *Brain Res. Bull.*, **31**, 565–572.

Collins, T.C., Petersen, N.J., Menke, T.J., Souchek, J., Foster, W. & Ashton, C.M. (2003) Short-term, intermediate-term, and long-term mortality in patients hospitalized for stroke. *J. Clin. Epidemiol.*, **56**, 81–87.

Conde, J.R. & Streit, W.J. (2006) Microglia in the aging brain. *J. Neuropathol. Exp. Neurol.*, **65**, 199–203.

Damoiseaux, J.G., Dopp, E.A., Calame, W., Chao, D., MacPherson, G.G. & Dijkstra, C.D. (1994) Rat macrophage lysosomal membrane antigen recognized by monoclonal antibody ED1. *Immunology*, **83**, 140–147.

Felberg, R.A., Grotta, J.C., Shirzadi, A.L., Strong, R., Narayana, P., Hill-Felberg, S.J. & Aronowski, J. (2002) Cell death in experimental intracerebral hemorrhage: the 'black hole' model of hemorrhagic damage. *Ann. Neurol.*, **51**, 517–524.

Fiala, M., Lin, J., Ringman, J., Kermani-Arab, V., Tsao, G., Patel, A., Lossinsky, A.S., Graves, M.C., Gustavson, A., Sayre, J., Sofroni, E., Suarez, T., Chiappelli, F. & Bernard, G. (2005) Ineffective phagocytosis of amyloid-beta by macrophages of Alzheimer's disease patients. *J. Alzheimers Dis.* , **7**, 221–232.

Fordyce, C.B., Jagasia, R., Zhu, X. & Schlichter, L.C. (2005) Microglia Kv1.3 channels contribute to their ability to kill neurons. *J. Neurosci.*, **25**, 7139–7149.

Franke, C.L., van Swieten, J.C. & van, G.J. (1991) Residual lesions on computed tomography after intracerebral hemorrhage. *Stroke*, **22**, 1530–1533.

Futrell, N., Garcia, J.H., Peterson, E. & Millikan, C. (1991) Embolic stroke in aged rats. *Stroke*, **22**, 1582–1591.

Gehrmann, J., Bonnekoh, P., Miyazawa, T., Hossmann, K.A. & Kreutzberg, G.W. (1992) Immunocytochemical study of an early microglial activation in ischemia. *J. Cereb. Blood Flow Metab.*, **12**, 257–269.

Gong, Y., Hua, Y., Keep, R.F., Hoff, J.T. & Xi, G. (2004) Intracerebral hemorrhage: effects of aging on brain edema and neurological deficits. *Stroke*, **35**, 2571–2575.

Hanisch, U.K. (2002) Microglia as a source and target of cytokines. *Glia*, **40**, 140–155.

He, Z., Crook, J.E., Meschia, J.F., Brott, T.G., Dickson, D.W. & McKinney, M. (2005) Aging blunts ischemic-preconditioning-induced neuroprotection following transient global ischemia in rats. *Curr. Neurovasc. Res.* , **2**, 365–374.

Kaushal, V., Koeberle, P.D., Wang, Y. & Schlichter, L.C. (2007) The Ca^{2+}-activated K^+ channel KCNN4/KCa3.1 contributes to microglia activation and nitric oxide-dependent neurodegeneration. *J. Neurosci.*, **27**, 234–244.

Koeppen, A.H., Dickson, A.C. & McEvoy, J.A. (1995) The cellular reactions to experimental intracerebral hemorrhage. *J. Neurol. Sci.*, **134**(Suppl.), 102–112.

Kreutzberg, G.W. (1996) Microglia: a sensor for pathological events in the CNS. *Trends Neurosci.*, **19**, 312–318.

Kullberg, S., Aldskogius, H. & Ulfhake, B. (2001) Microglial activation, emergence of ED1-expressing cells and clusterin upregulation in the aging rat CNS, with special reference to the spinal cord. *Brain Res.*, **899**, 169–186.

Lee, J.C., Cho, G.S., Choi, B.O., Kim, H.C., Kim, Y.S. & Kim, W.K. (2006) Intracerebral hemorrhage-induced brain injury is aggravated in senescence-accelerated prone mice. *Stroke*, **37**, 216–222.

Lehrmann, E., Christensen, T., Zimmer, J., Diemer, N.H. & Finsen, B. (1997) Microglial and macrophage reactions mark progressive changes and define the penumbra in the rat neocortex and striatum after transient middle cerebral artery occlusion. *J. Comp. Neurol.*, **386**, 461–476.

Lopes, K.O., Sparks, D.L. & Streit, W.J. (2008) Microglial dystrophy in the aged and Alzheimer's disease brain is associated with ferritin immunoreactivity. *Glia*, **56**, 1048–1060.

MacLellan, C.L., Girgis, J. & Colbourne, F. (2004) Delayed onset of prolonged hypothermia improves outcome after intracerebral hemorrhage in rats. *J. Cereb. Blood Flow Metab.*, **24**, 432–440.

MacLellan, C.L., Davies, L.M., Fingas, M.S. & Colbourne, F. (2006) The influence of hypothermia on outcome after intracerebral hemorrhage in rats. *Stroke*, **37**, 1266–1270.

MacLellan, C.L., Silasi, G., Poon, C.C., Edmundson, C.L., Buist, R., Peeling, J. & Colbourne, F. (2008) Intracerebral hemorrhage models in rat: comparing collagenase to blood infusion. *J. Cereb. Blood Flow Metab.*, **28**, 516–525.

Masada, T., Hua, Y., Xi, G., Yang, G.Y., Hoff, J.T. & Keep, R.F. (2001) Attenuation of intracerebral hemorrhage and thrombin-induced brain edema by overexpression of interleukin-1 receptor antagonist. *J. Neurosurg.*, **95**, 680–686.

Masoro, E.J. (1980) Mortality and growth characteristics of rat strains commonly used in aging research. *Exp. Aging Res.*, **6**, 219–233.

Mayer, S.A. & Rincon, F. (2005) Treatment of intracerebral haemorrhage. *Lancet Neurol.* , **4**, 662–672.

Mayne, M., Fotheringham, J., Yan, H.J., Power, C., Del Bigio, M.R., Peeling, J. & Geiger, J.D. (2001a) Adenosine A2A receptor activation reduces proinflammatory events and decreases cell death following intracerebral hemorrhage. *Ann. Neurol.*, **49**, 727–735.

Mayne, M., Ni, W., Yan, H.J., Xue, M., Johnston, J.B., Del Bigio, M.R., Peeling, J. & Power, C. (2001b) Antisense oligodeoxynucleotide inhibition of tumor necrosis factor-alpha expression is neuroprotective after intracerebral hemorrhage. *Stroke*, **32**, 240–248.

Nimmerjahn, A., Kirchhoff, F. & Helmchen, F. (2005) Resting microglial cells are highly dynamic surveillants of brain parenchyma in vivo. *Science*, **308**, 1314–1318.

O'Donnell, H.C., Rosand, J., Knudsen, K.A., Furie, K.L., Segal, A.Z., Chiu, R.I., Ikeda, D. & Greenberg, S.M. (2000) Apolipoprotein E genotype and the risk of recurrent lobar intracerebral hemorrhage. *N. Engl. J. Med.*, **342**, 240–245.

Peeling, J., Del Bigio, M.R., Corbett, D., Green, A.R. & Jackson, D.M. (2001) Efficacy of disodium 4-[(tert-butylimino)methyl]benzene-1, 3-disulfonate N-oxide (NXY-059), a free radical trapping agent, in a rat model of hemorrhagic stroke. *Neuropharmacology*, **40**, 433–439.

Popa-Wagner, A., Schroder, E., Walker, L.C. & Kessler, C. (1998) beta-Amyloid precursor protein and ss-amyloid peptide immunoreactivity in the rat brain after middle cerebral artery occlusion: effect of age. *Stroke*, **29**, 2196–2202.

Power, C., Henry, S., Del Bigio, M.R., Larsen, P.H., Corbett, D., Imai, Y., Yong, V.W. & Peeling, J. (2003) Intracerebral hemorrhage induces macrophage activation and matrix metalloproteinases. *Ann. Neurol.*, **53**, 731–742.

Rincon, F. & Mayer, S.A. (2004) Novel therapies for intracerebral hemorrhage. *Curr. Opin. Crit. Care*, **10**, 94–100.

Rosenberg, G.A., Mun-Bryce, S., Wesley, M. & Kornfeld, M. (1990) Collagenase-induced intracerebral hemorrhage in rats. *Stroke*, **21**, 801–807.

Schilling, M., Besselmann, M., Muller, M., Strecker, J.K., Ringelstein, E.B. & Kiefer, R. (2005) Predominant phagocytic activity of resident microglia over hematogenous macrophages following transient focal cerebral ischemia: an investigation using green fluorescent protein transgenic bone marrow chimeric mice. *Exp. Neurol.*, **196**, 290–297.

Schmued, L.C. & Hopkins, K.J. (2000) Fluoro-Jade B: a high affinity fluorescent marker for the localization of neuronal degeneration. *Brain Res.*, **874**, 123–130.

Simmons, D.A., Casale, M., Alcon, B., Pham, N., Narayan, N. & Lynch, G. (2007) Ferritin accumulation in dystrophic microglia is an early event in the development of Huntington's disease. *Glia*, **55**, 1074–1084.

Streit, W.J. (2002) Microglia as neuroprotective, immunocompetent cells of the CNS. *Glia*, **40**, 133–139.

Streit, W.J., Sammons, N.W., Kuhns, A.J. & Sparks, D.L. (2004) Dystrophic microglia in the aging human brain. *Glia*, **45**, 208–212.

Wang, J. & Tsirka, S.E. (2005a) Tuftsin fragment 1-3 is beneficial when delivered after the induction of intracerebral hemorrhage. *Stroke*, **36**, 613–618.

Wang, J. & Tsirka, S.E. (2005b) Neuroprotection by inhibition of matrix metalloproteinases in a mouse model of intracerebral haemorrhage. *Brain*, **128**, 1622–1633.

Wang, J., Rogove, A.D., Tsirka, A.E. & Tsirka, S.E. (2003) Protective role of tuftsin fragment 1-3 in an animal model of intracerebral hemorrhage. *Ann. Neurol.*, **54**, 655–664.

Wasserman, J.K. & Schlichter, L.C. (2007a) Neuron death and inflammation in a rat model of intracerebral hemorrhage: effects of delayed minocycline treatment. *Brain Res.*, **1136**, 208–218.

Wasserman, J.K. & Schlichter, L.C. (2007b) Minocycline protects the blood-brain barrier and reduces edema following intracerebral hemorrhage in the rat. *Exp. Neurol.*, **207**, 227–237.

Wasserman, J.K., Zhu, X. & Schlichter, L.C. (2007) Evolution of the inflammatory response in the brain following intracerebral hemorrhage and effects of delayed minocycline treatment. *Brain Res.*, **1180**, 140–154.

Xue, M. & Del Bigio, M.R. (2001) Acute tissue damage after injections of thrombin and plasmin into rat striatum. *Stroke*, **32**, 2164–2169.

Zhao, X., Sun, G., Zhang, J., Strong, R., Song, W., Gonzales, N., Grotta, J.C. & Aronowski, J. (2007) Hematoma resolution as a target for intracerebral hemorrhage treatment: role for peroxisome proliferator-activated receptor gamma in microglia/macrophages. *Ann. Neurol.*, **61**, 352–362.